Article:

Alzraiee, A.H., Bailey, R. and Bau, D. orcid.org/0000-0002-0730-5478 (2017) Assimilation of Historical Head Data to Estimate Spatial Distributions of Stream Bed and Aquifer Hydraulic Conductivity Fields. Hydrological Processes, 31 (7). pp. 1527-1538. ISSN 0885-6087

https://doi.org/10.1002/hyp.11123

Assimilation of Historical Head Data to Estimate Spatial Distributions of Stream Bed and Aquifer Hydraulic Conductivity Fields

Ayman H. Alzraiee[1*], Ryan Bailey[2], Domenico Bau[3]

[1*] Dept. of Civil and Environmental Engineering (1372), Colorado State Univ., Fort Collins, CO. 80523, Email: ayman.alzraiee@gmail.com

[2] Dept. of Civil and Environmental Engineering (1372), Colorado State Univ., Fort Collins, CO. 80523, Email: rtbailey@engr.colostate.edu

[3] Department of Civil and Structural Engineering, University of Sheffield, Sheffield, UK, Email: d.bau@sheffield.ac.uk

*Corresponding author:

Email: ayman.alzraiee@gmail.com

Tel: 970-286-4380

September 2016

Accepted version.

Published in: **Hydrological Processes, Volume 31, Issue 7, 30 March 2017, pp. 1527–1538**

Abstract

Management of water resources in alluvial aquifers relies mainly on understanding interactions between hydraulically connected streams and aquifers. Numerical models that simulate this interaction often are used as decision support tools in water resource management. However, the accuracy of numerical predictions relies heavily on the unknown system parameters (i.e. stream bed conductivity and aquifer hydraulic conductivity) which are spatially heterogeneous and difficult to measure directly. This paper employs an Ensemble Smoother to invert groundwater level measurements to jointly estimate spatially-varying streambed and alluvial aquifer hydraulic conductivity along a 35.6 km segment of the South Platte River in northeastern Colorado. The accuracy of the inversion procedure is evaluated using a synthetic experiment and historical groundwater level measurements, with the latter constituting the novelty of this study in the inversion and validation of high resolution fields of streambed and aquifer conductivities. Results show that the estimated streambed conductivity field and aquifer conductivity field produce an acceptable agreement between observed and simulated groundwater levels and stream flow rates. The estimated parameter fields are also used to simulate the spatially varying flow exchange between the alluvial aquifer and the stream, which exhibit high spatial variability along the river reach with a maximum average monthly aquifer gain of about 2.3 m^3/day and a maximum average monthly aquifer loss of 2.8 m^3/day, per unit area of streambed (m^2). These results demonstrate that data assimilation inversion provides a reliable and computationally affordable tool to estimate the spatial variability of streambed and aquifer conductivities at high resolution in real-world systems.

1. Introduction

Exchange of water between groundwater systems and surface water systems can have a significant impact on biogeochemical nutrient cycling in the hyporheic zone (Frei et al., 2009; Kurtz et al., 2012), riparian zone ecology (Cey et al., 1999) and processes (e.g. vegetation growth, nutrient flux), environmental flows and associated habitat quality, mass flux of solutes between aquifer and streams (Hussein and Schwartz, 2003; Kalbus et al., 2007), and the general water balance of the stream-aquifer system (Frei et al., 2009; Kurtz et al., 2012). For the latter, water management practices can be dependent on groundwater-surface water exchange, for example significant groundwater recharge in losing reaches of a stream or stream depletion due to nearby alluvial groundwater pumping (Glover and Balmer, 1954; Jenkins, 1968; Sophocleous et al., 1995; Chen and Shu, 2002; Miller et al., 2007).

Fluxes between groundwater and surface water, either through groundwater discharge to streams or stream water seepage into aquifers, are governed by the position of stream stage with respect to the water table, the geometry and position of the stream channel within the alluvial plain, and the hydraulic properties of the aquifer and the streambed (Woessner, 2000; Cardenas et al., 2004). Of these, hydraulic conductivity (K_s) of streambed sediments along the aquifer-stream interface often is the principal control, with exchange fluxes often being highly spatially variable (sometimes on the order of meters to centimeters) due to strong spatial heterogeneity of streambed K_s (Fleckenstein et al., 2006; Frei et la., 2009; Kalbus et al., 2009; Rosenberry and Pitlick, 2009; Vogt et al., 2010). Streambed K_s can range over orders of magnitude (Calver, 2001) over relatively short (0.2 km to 10 km) reaches of a stream (Genereux et al. 2008; Hatch et al,. 2010). Heterogeneity of aquifer properties also can have a strong impact on stream-aquifer exchange (Kalbus et al., 2009). In general, assuming complete or partial spatial uniformity in streambed K_s can yield erroneous estimates of groundwater discharge and stream flow depletion (Kurtz et al., 2013; Lackey et al., 2015), with important implications for water management in coupled stream-aquifer systems. As such, a key objective in investigating groundwater-surface interactions is an accurate estimation of spatially-varying streambed K_s along a river reach.

Numerous methods have been employed to estimate spatially-variable streambed K_s, with the overall goal of providing reliable estimates of exchange flux in space and time. These methods include permeameter tests and seepage meters (Avery, 1994; Duff et al., 2000; Paulsen et al., 2001); electrical resistivity surveys of streambed sediment (Nyquist et al., 2008); streambed temperature mapping, vertical temperature profiling and heat transport modeling (Silliman and Booth, 1993; Silliman et al., 1995; Fryar et al, 2000; Becker et al., 2004; Keery et al., 2007; Vogt et al., 2010; Kurtz et al., 2014); water balance approaches (Krause et al., 2007); and the use of numerical groundwater models (Morway et al., 2013) or coupled surface-subsurface hydrologic models (Frei et al., 2009). For numerical models, streambed K_s is varied spatially to provide matches between observed and simulated hydraulic head data and stream stage data. As identified in recent studies, there is a need to assess streambed K_s at larger scales (i.e. longer reaches of streams) (Frei et al., 2009) while still targeting sufficient spatial resolution (Fleckenstein et al., 2010).

As an alternative to these methods, numerical hydrologic modeling coupled with data assimilation methods can be used to estimate spatially-varying streambed K_s along the stream-aquifer interface. Data assimilation methods such as the Kalman Filter and variants such as the Ensemble Kalman Filter (EnKF) (Evensen, 1994; Burgers et al., 1998) and the Ensemble Smoother (ES) (van Leeuwen and Evensen, 1996) have been used in numerous hydrologic studies to estimate aquifer hydraulic conductivity and transmissivity (Hantush and Marino, 1997;

Chen and Zhang, 2006; Hendricks Franssen and Kinzelbach, 2008; Alzraiee et al., 2014), first-order reaction rates of solutes (Bailey and Baù, 2011; Bailey et al., 2013), and aquifer dispersivity (Wagner, 1992; Lui et al., 2008). In these methods, system-response variables (e.g. groundwater hydraulic head, groundwater solute concentration) and system parameters (e.g. streambed conductance and hydraulic conductivity field) are jointly updated by assimilating measurement data from the true state.

Several recent studies (Hendricks Franssen et al., 2011; Kurtz et al., 2012; Kurtz et al., 2013), all applied to the Limmat Aquifer system near Zurich, Switzerland, used the EnKF to jointly update aquifer hydraulic conductivity, K_a , and streambed K_s. Using a variably saturated groundwater flow model with stream-aquifer interactions, Hendricks Franssen et al. (2011) and Kurtz et al. (2012) estimated stream leakage coefficients in five zones by assimilating hydraulic head data, with the latter study estimating temporal-varying stream bed K_s. Kurtz et al. (2013) estimated stream bed K_s in a synthetic system in settings of varying degrees of heterogeneity, ranging from two K_s zones to a fully heterogeneous system wherein each stream node received a different value of K_s.

The overall objective of this study is to jointly estimate the spatial variability of streambed conductivity, K_s, and aquifer conductivity, K_a, at relatively high resolutions (304.8 m) within a regional-scale river-aquifer system using historical data. Specifically, the Ensemble Smoother (ES) (van Leeuwen and Evensen, 1996) is used to estimate spatially-varying fields of aquifer K_a and streambed K_s within a 35.6 km reach of the South Platte River in northeastern Colorado via assimilation of time series of hydraulic head data from nearby observation wells. Following a demonstrative example using synthetic head data, historical measurements are used to estimate the parameter fields. The performance of the parameter inversion is evaluated using historical data from observation wells not used in parameter estimation, and the posterior uncertainty in the predicted stream-aquifer flux exchanges are quantified.

To our knowledge, this is the first study to use an Ensemble Smoother to assimilate historical hydraulic head data to estimate and corroborate strongly heterogeneous streambed K_s and aquifer K_a. The methodology presented herein can be transferred to stream-aquifer systems in other alluvial river valleys.

2. Site Description

The South Platte Basin (Figure 1) covers approximately 21% of the State of Colorado (about 57,000 km^2), within which the South Platte River Basin alluvial groundwater system constitutes 19% (about 10,400 km^2) (Colorado Geological Survey 2003). As of 2008, the irrigated farmland was 335,000 ha, to support a population of 3.5 million (CDM Smith, 2013).

The surface hydrological system consists of the main stem of the South Platte River and its tributaries (Figure 1B). The alluvial deposits in the South Platte Basin consist mainly of sand and gravels. The alluvial aquifer is believed to be hydraulically connected to the surface water system throughout much of the basin (CDM Smith, 2013). The saturated thickness of the alluvial aquifer generally increases along the downstream direction (west to east), with saturated aquifer thicknesses ranging between 6 and 90 m. The aquifer hydraulic conductivity K_a ranges between approximately 30 and 600 m/day, depending on the degree of sorting and the amount of fine grain material present (CDM Smith, 2013). Agricultural irrigation is the dominant water use in the South Platte River Basin (CDM Smith, 2013).

In a joint effort of the Colorado Water Conversation Board and the Colorado Division of Water Resources (DWR) and as a part of the South Platte Decision Support System (SPDSS), a large-scale regional groundwater model based on MODFLOW (Harbaugh et al. 2000) was developed and calibrated for a large portion of the alluvial aquifer by CDM Smith (2013). The modeled area (Figure 1A) is about 63% of the alluvial aquifer (6,400 km^2), and the simulation time period is between 1950 and 2006. More information about the model is provided in Section 4.

In this paper and for the purpose of high-resolution parameter estimation, we focus on a smaller portion of the alluvial aquifer as shown in Figure 1B. The simulated area extends over 30 km in the east-west direction along the South Platte River between the towns of Snyder and Atwood. The length of the river stem in the study area is about 35.6 km.

3. Methodology

3.1 Formulation of the Inverse Problem

The rate of flux exchange between streams network and aquifer depends largely on the difference between stream stage and local water table elevation. The numerical simulation of this interaction is based on coupling the groundwater continuity equation with the stream water continuity and momentum equations. This coupling is achieved in MODFLOW's Streamflow-Routing (SFR) package (Prudic et al. 2004) by calculating the stream depth at the midpoint of each reach and assuming uniform flow between streams and aquifer over a given section of the stream and the corresponding volume of aquifer. Streamflow routing in SFR is modeled using the continuity equation and by assuming that streamflow is steady in discrete time periods, and uniform within each numerical cellblock.

Depending on the elevation of stream stage with respect to the elevation of the water table in the local aquifer, a stream can be either gaining or losing. The stream is gaining when the water table is above the stream stage elevation; in this case, the exchange flow rate is computed as:

$$Q_{sa} = \frac{K_s wL}{m}\left(h_s - h_a\right) \qquad (1)$$

where Q_{sa} is the water exchange flow rate between a given section of the stream and the local aquifer [L^3T^{-1}], K_s is the hydraulic conductivity of the streambed sediments [$L\ T^{-1}$], w is the stream width [L], L is the stream length in the finite difference cell [L], m is the thickness of stream bed deposits [L], h_s is the head in the stream [L], and h_a is the head in the aquifer beneath the streambed [L]. When the water table is below the streambed elevation, MODFLOW-SFR package assumes that water exchange flow rate is independent of h_a. In this case, the stream-aquifer flow is calculated by assuming head difference equal to the streambed thickness.

Assuming a constant streambed thickness in Equation (1), K_s and h_a (controlled by the K_a field) are the principle controlling factors of water exchange rate, and are spatially heterogeneous fields that cannot be uniquely determined from a finite number of field samples and associated parameter measurements. Alternatively, inverse modeling allows incorporating relatively low cost measurements of water table elevation and stream flow rate to predict these parameters.

To simplify the illustration of inverse modeling for this problem, consider the following generic model that relates an observable vector **d** to a vector of high-dimensional input parameters **m**,

$$\mathbf{d} = \mathbf{G}\left(\mathbf{m}\right) \qquad (2)$$

where **d** is $n_d \times 1$ vector that encompasses predicted states (e.g. hydraulic heads h_x^t) at a set of observable spatial locations x and at a set of times t; **m** is a vector with dimension $n_m \times 1$ that encompasses system parameters that controls observable states, and **G** is a generic flow model that maps input parameters to observable states.

In this study, we assume that uncertainty in stream-aquifer interaction is mainly attributed to the unknown streambed K_s and aquifer K_a fields. Other factors affecting the interactions, such as groundwater stresses and boundary conditions, are determined from field measurements and the calibrated regional model as discussed in Section 4.1. Thus, the vector of parameters to be determined can be written as $\mathbf{m}=[K_s,\ K_a]^T$.

Inverse modeling of high-dimensional parameters is usually affected by the problem of non-uniqueness (Beven 2001), which occurs when a small number of observations are used to estimate a larger number of system parameters. For this situation, an infinite number of solutions to the inverse problem are possible. More realistically, all possible parameter solutions fitting to a probability distribution function (PDF) conditional to a set of observations may be described using Bayes' law:

$$P(\mathbf{m}\,|\,\mathbf{d}_{\mathrm{o}})=\frac{P(\mathbf{d}_{\mathrm{o}}\,|\,\mathbf{m})P\left(\mathbf{m}\right)}{P\left(\mathbf{d}_{\mathrm{o}}\right)} \qquad (3)$$

where $P(\mathbf{m}\,|\,\mathbf{d}_{\mathrm{o}})$ is the posterior probability of model parameters **m** given a vector of observations $\mathbf{d}_{\mathrm{o}}$, $P(\mathbf{d}_{\mathrm{o}}\,|\,\mathbf{m})$ is the likelihood probability distribution, P(**m**) is the prior model parameter distribution, and P($\mathbf{d}_{\mathrm{o}}$) is a normalization term.

One of the few analytical solutions that can be obtained from Bayes' law occurs when the forward model **G** is linear and the PDF of system parameters in Equation (3) is multivariate Gaussian, $P\left(\mathbf{m}\right)\sim N\left(\bar{\mathbf{m}},\mathbf{C}_m\right)$, where $\bar{\mathbf{m}}$ is the prior mean of parameters vector and $\mathbf{C}_{\mathrm{m}}$ is the parameter prior covariance matrix. In this case, the posterior distribution also follows a Gaussian distribution, i.e. $P\left(\mathbf{m}|\mathrm{d}_{\mathrm{o}}\right)\sim N\left(\hat{\mathbf{m}},\hat{\mathbf{C}}_m\right)$, where the posterior mean vector and posterior covariance matrix are computed as follows:

$$\hat{\mathbf{m}} = \bar{\mathbf{m}} + \mathbf{C}_{md}\mathbf{C}_{dd}^{\;1}\left(\mathbf{d}_{o} \quad \bar{\mathbf{m}}\right) \qquad (4)$$

$$\hat{\mathbf{C}}_{m} = \mathbf{C}_{m} - \mathbf{C}_{md}\mathbf{C}_{dd}^{-1}\mathbf{C}_{md} \qquad (5)$$

where $\hat{\mathbf{m}}$ is the mean of the posterior Gaussian PDF of system parameters, $\mathbf{C}_{md}$ is a $n_m \times n_d$ matrix that describes the cross-covariance between system parameters and observable states, $\mathbf{C}_{dd}$ is the auto-covariance matrix of the observable states and has a dimension of $n_d \times n_d$, and $\hat{\mathbf{C}}_{m} \in n_m \times n_m$ is the posterior covariance matrix of system parameters.

In practice, the assumptions of model linearity and parameter Gaussianity restrict the wide applications of this formulation. Additionally, it is computationally intensive to compute the parameter-state cross-covariance matrix for high-dimensional models. Evensen (1994) proposed an ensemble-based formulation of the Kalman Filter for high-dimensional problems. In this formulation, the prior PDF is approximated using an ensemble of parameter-state realizations produced through a Monte Carlo simulation by:

$$\mathbf{X}_{p} = \begin{bmatrix} \mathbf{m}_{1} & & \mathbf{m}_{N} \\ \mathbf{d}_{1} & \dots & \mathbf{d}_{N} \end{bmatrix} \qquad (6)$$

where N is the number of realizations in the ensemble and $\mathbf{X}_p$ is the parameter-state forecast (prior) matrix with dimensions $(n_m + n_d) \times N$. Using this matrix, the prior ensemble covariance matrix can be calculated as

$$\mathbf{C}_{p} = \frac{(\mathbf{X}_{p} - \hat{\mathbf{X}}_{p})(\mathbf{X}_{p} - \hat{\mathbf{X}}_{p})^{\mathbf{T}}}{N - 1} \qquad (7)$$

where $\hat{\mathbf{X}}_{\mathbf{p}}$ is a matrix with dimension $(\mathrm{n_m}+\mathrm{n_d})\times\mathrm{N}$ where each column is the prior ensemble mean vector. Following Equations (4) and (5), the update forecast matrix and update covariance matrix can be written as follows:

$$\mathbf{X}_{\mathrm{u}}=\mathbf{X}_{\mathrm{p}}+\mathbf{\Phi}\left(\mathbf{D}-\mathbf{H}\mathbf{X}_{\mathrm{p}}\right) \qquad (8)$$

$$\mathbf{C}_{\mathrm{u}}=\left(\mathbf{I}-\mathbf{K}\mathbf{H}\right)\mathbf{C}_{\mathrm{p}} \qquad (9)$$

where $\mathbf{X}_{\mathrm{u}}$ is the update parameter-state matrix, **D** is the perturbed measurements matrix with dimension $\mathrm{n_d}\times\mathrm{N}$, **H** is a binary matrix ($\mathrm{n_d}\times\mathrm{n_m}$) that is used to extract model predictions at locations and times of observations data, $\mathbf{C}_{\mathrm{u}}$ is the update covariance matrix and **I** is the identity matrix. $\mathbf{\Phi}$ is the so-called Kalman Gain matrix ($\mathrm{n_m}\times\mathrm{n_d}$), computed as:

$$\mathbf{\Phi}=\mathbf{C}_{\mathrm{p}}\mathbf{H}^{\mathrm{T}}(\mathbf{H}\mathbf{C}_{\mathrm{p}}\mathbf{H}^{\mathrm{T}}+\mathbf{R})^{-1} \qquad (10)$$

In equation (10), **R** is the covariance matrix $\mathrm{n_d}\times\mathrm{n_d}$ of measurement errors computed from uncorrelated error realizations generated from $\sim\mathrm{N}\left(0,\sigma_{\mathrm{e}}\right)$, where σ_{e} is the error standard deviation that reflects confidence in measurements. When the observation vector $\mathbf{d}_{\mathrm{o}}$ incorporates data at multiple times, i.e. $\mathbf{d}_o=\left\lfloor \mathbf{d}_{t=1}, \quad ,\mathbf{d}_{t=n_t}\right\rfloor$, the objective of the Bayesian update is to compute the posterior distribution $P(\mathbf{m}\,|\,\mathbf{d}_{t=1}, \quad ,\mathbf{d}_{t=n_t})$, where $\mathrm{n_t}$ is the number of temporal measurements. For this situation, it is straightforward to expand the Ensemble Kalman Filter to the Ensemble Smoother (ES) (van Leeuwen and Evensen, 1996) that assimilates all available measurements from any time into a single update step. To implement the ES, the forecast matrix incorporates parameters and model responses at all observable locations and times as follows:

$$\mathbf{X}_p = \begin{bmatrix} \mathbf{m}_1 & \cdots & \mathbf{m}_N \\ \mathbf{d}_1^{t=1} & & \mathbf{d}_N^{t=1} \\ \vdots & \cdots & \vdots \\ \mathbf{d}_1^{t=n_t} & & \mathbf{d}_N^{t=n_t} \end{bmatrix} \qquad (11)$$

The forecast matrix in Equation (11) is used to calculate the spatio-temporal cross-covariance matrix using Equation (7). Similar to the EnKF, Equations (8) to (10) can be used to achieve the update in ES**.**

4. Application

4.1 Model Settings and Field Observations

The model input data are extracted from the regional SPDSS MODFLOW groundwater model (CDM Smith, 2013). The numerical model domain consists of a single layer and 100 columns and 100 rows. Each cell is 304.8 m x 304.8 m (1000 ft). The saturated thickness in the simulated area ranges between 60 m to 88 m along the river pathway and decreases away from the river to a minimum of about 15 m along the edges of the alluvial aquifer.

The extracted simulated period spans from 2000 to 2006. The system stresses include: (a) spatially variable recharge, accounting for deep percolation resulting from precipitation, irrigation return flow, and seepage from ditches and canals (CDM Smith, 2013); (b) spatially variable evapotranspiration (ET) computed internally by the MODFLOW-ETS package as a function of groundwater depth and measured reference ET; and (c) about 500 pumping and injection wells with flow rates changing seasonally. The system stresses change monthly to allow for seasonal variation. Thus, the simulation period is divided into 84 transient state stress-periods and one steady-state simulation in the first month of 2000.

The upstream and downstream boundary conditions are chosen to be Neumann-type time variable lateral flow conditions. The monthly groundwater lateral flow rates are extracted from the regional groundwater flow model using a zonal mass balance analysis for the study area, resulting in a generally west-to-east flow regime (Figure 2). The boundary conditions on the northern and southern sides of the model are simulated to be variable flux and are obtained from the regional groundwater model as well.

4.2 Numerical Experiments

Implementing Data Assimilation techniques for system parameter estimation is performed in two stages: a forecast or simulation stage, and an update or assimilation stage.

In the first stage (forecast), a Monte Carlo simulation is conducted in which a number of realizations of streambed K_s and the aquifer K_a fields are generated and processed in the flow model. To generate prior realizations, $\mathrm{y} = \log\left(\mathrm{K_a}\right)$ is assumed to fit to an isotropic and stationary Gaussian process (de Marsily 1986) with a prescribed covariance model $C_{yy}\left(d;\ {}_{y},\ {}^{2}_{y}\right)$. Similarly, $\mathrm{z} = \log\left(\mathrm{K_s}\right)$ is assumed to fit to a one-dimensional correlated random process representing the spatial variability of streambed conductivity $C_{zz}\left(d;\ {}_{z},\ {}^{2}_{z}\right)$ along the stream pathway. The parameters λ and σ^2 represent the correlation length [L] and the variance of the random processes, respectively. The stationary means of the two fields are μ_y and μ_z.

Table 1 summarizes the geostatistical properties of the two fields. In this study, a spherical covariance function is assumed for both C_{yy} and C_{zz}, yet other covariance functional forms can also be used. The number of generated realizations for both K_s and K_a fields is 500. The range of spatial variability of the specific yield is typically narrow, thus this parameter is assumed homogenous with a value of 0.2 (CDM Smith, 2013).

In the second stage (update), the system parameters and states are updated using Equations 8 and 9. The update ensemble can be used to quantify the uncertainty in posterior estimates.

Two sets of experiments are performed in this study (Table 2). The first experiment, termed A, provides an initial test of the methodology by assimilating synthetic hydraulic head values generated from a flow model that simulates known reference K_s and K_a fields. The spatial locations and times of the synthetic observations are the same as those of the available historical observations. The purpose of choosing this spatio-temporal configuration of synthetic observations is to evaluate possible biases in inversion results introduced from the number of observations and their spatio-temporal distribution. The objective of this experiment is to test the ability of the ensemble smoother (ES) to estimate the true K_s and K_a fields using only hydraulic head data.

To evaluate the performance of inverse parameter estimations in experiment A, the estimated parameter fields are compared with referenced ones using two performance statistics: (1) the mean absolute error L_1, and Pearson's correlation coefficient r, which are respectively calculated as follows:

$$L_1 = \frac{1}{n}\sum_{i=1}^{i=n}\left|\phi_{True}(i) - \phi_{est}(i)\right| \qquad (12)$$

$$r = \frac{\sum_{i=1}^{n}\left[\phi_{true}(i) - \overline{\phi_{true}}\right]\cdot\left[\phi_{est}(i) - \overline{\phi_{est}}\right]}{\sqrt{\sum_{i=1}^{n}\left[\phi_{true}(i) - \overline{\phi_{true}}\right]^2 \cdot \sum_{i=1}^{n}\left[\phi_{est}(i) - \overline{\phi_{est}}\right]^2}} \qquad (13)$$

where ϕ_{true} is the true (or reference) parameter vector and ϕ_{est} is the estimate parameter vector. The Pearson's correlation coefficient r provides a measure for the linear correlation between the estimated and the reference parameter vectors.

Experiment B-1 assimilates historical groundwater level data collected from the field. Figure 2 shows the locations of the 16 observations wells used in the assimilation. The temporal span of data varies from well to well within the period 2000-2006. The total number of water table measurements from the 16 wells is 4,944. Only half of the available water table elevation data are assimilated, in particular those collected during the first half of the 2000-2006 period.

In experiment B-2, results of experiment B-1 are validated by comparing observed states (water table elevation and streamflow) with states obtained numerically by simulating the updated K_s and K_a fields. Comparisons are carried out using Equations 12 and 13, with ϕ representing groundwater hydraulic head or streamflow. In this analysis, only water table elevation data collected in the second half of the 2000-2006 period are used. The comparison is also carried out with respect to streamflow rates observed at a stream gage located 6 km from the upstream end of the model domain (Figure 2). Note that, due to the relative proximity of the stream flow gauge to the upstream end, the contribution of aquifer losses or gains to the South Platte River is relatively small. Therefore, streamflow data was not used in updating parameter fields.

5. Results and Discussion

5.1 Assimilation of Synthetic Hydraulic Head Data

Figure 3 shows the reference streambed K_s field and the mean of the K_s fields as updated by assimilating synthetic hydraulic head data in experiment A. The two fields are very close in magnitude and patterns of spatial variation. Figure 4 shows a scatter plot of the updated mean and reference K_s fields in relation to a 1-1 line. The correlation between the two fields is high with r = 0.98 and L_1 = 0.0379 (Equations 12 and 13), indicating that when system stresses are known, the streambed K_s field can be estimated effectively using hydraulic head data only. This notion can be understood by observing that Equation (1) relates aquifer water losses to the difference between head in the aquifer and stream stage. Since the uncertainty in stream stage is relatively smaller than the uncertainty in water table elevation (because stream-bed elevation can be directly measured and stage variability is typically small at the site), the uncertainty of flux depends largely on the adjacent aquifer head field, which is controlled principally by the spatial distribution of K_a. That is to say, the exchange flux rates between the aquifer and the river are governed mainly by the aquifer hydraulic head data. However, this situation likely is not realized in reality, since other sources of uncertainty, for example of conceptual and structural nature, can contribute to the prediction errors.

Figure 5 shows the reference K_a field and the mean of the updated K_a ensemble. A visual comparison shows that the two fields are very similar in values and spatial distribution. Figure 6 shows a scatter plot of the estimated and reference field with a 1-1 line. The correlation between the two fields is high with r = 0.98 and L_1 = 0.153 indicating a high performance of the ES in estimating the reference K_a field. It is important to recall that the hydraulic stresses used to generate the synthetic measurements are the same as those used to generate the realizations in the forecast state-parameter matrix, i.e. the discrepancy between the prior head ensemble and the synthetic measurements comes in this case only from the unknown system parameters.

5.2 Assimilation of Historical Groundwater Level Measurements (Experiment B-1)

Figure 7a shows the ensemble mean of the updated K_a fields from assimilating half of the available head data as in experiment B-1. The spatial variability of the estimated $\ln(K_a)$ ranges between 1 and 10 (ln(m/day)), which are reasonable values for an alluvial aquifer. To evaluate the efficiency of this estimate, the posterior standard deviation is plotted in Figure 7b. The posterior standard deviation ranges between 0.5 and 1.2 (ln(m/day)). These values correspond to coefficient of variations that range between 5.5% and 60%. A close analysis of the spatial distribution of the standard deviation of the updated K_a field reveals that regions of low standard deviation coincide with the locations of observation wells (Figure 2).

Figure 8 shows the prior and posterior ensembles of K_s. The posterior ensemble mean of streambed K_s is also shown. One can see that the prior ensemble mean is constant with a value of z = 0 (equivalent to 1 m/day), while the posterior mean is spatially variable. The posterior mean of ln(K_s) ranges between the values -0.5 and 0.5 (equivalent to 0.61-1.65 m/day), which are within the range of published conductivity values (0.01 to 85 m/day) published by Calver (2001).

One important observation is that the range of variability of the estimated K_s values is relatively small when compared to published values (Calver, 2001), which could have a wider range of 1-100 m/day at the same site. This can be explained by recalling that the cell size in the model is about 304.8 m and thus the resulting estimates are the effective stream conductivity on a support scale of about 304.8 m and stream width of 14 m. The sensitivity of calibration results to uncertainty in the prior standard deviation was investigated by repeating the calibration using different prior standard deviations (σ_z = 0.1, 1.0, 2.0). Results indicate that applying different standard deviations does not have a large effect on the posterior ensemble. These results are not shown here.

It is worth recalling that these results rely on the assumption that K_s is constant with time. A number of studies have shown that this is not always the case, as flood events and streambed erosion might introduce changes in magnitudes and spatial distribution of K_s (Springer et al., 1999; Cardenas et al. 2004). In this respect, the K_s estimates shown in Figure 8 represent "effective" K_s values over the period 2000-2006.

The statistical properties of the total stream-aquifer flux exchange along the simulated reach (about 35.6 km long) are summarized in Figure 9, which shows the prior and posterior distribution of the total flux. Flow values are calculated for each of the 500 realizations by temporally averaging (over 84 months stress periods) the total stream exchange flow between the 35.6 km river and the aquifer. Both prior and posterior average total flows are negative which indicate the case of an aquifer discharging groundwater to the stream (gaining stream), which is expected according to common understanding of the South Platte River interaction with the alluvial aquifer. The prior mean total flow is about -0.83×10^5 m^3/day and the posterior mean is -1.34×10^6 m^3/day. These values are equivalent to 2.33 m^3/day per unit length of the stream for the prior flow and 4.01 m^3/day per unit length of the stream for the posterior flow.

To gain more insight on the spatial distribution of flux exchange, Figure 10 shows the posterior ensemble and the posterior ensemble mean of the stream-aquifer flux along the length of the South Platte River. While the flow in general is from the aquifer to the stream, some segments experience flow from the stream to the aquifer. The spatial variability along the river reach has a maximum average monthly aquifer gain of about 0.98×10^4 m^3/day/per stream reach (2.3 m^3/day/m^2) and a maximum average monthly aquifer loss of 1.2×10^4 m^3/day/per stream reach (2.8 m^3/day/m^2).

5.3 Validation of Assimilation Results (Experiment B-2)

As indicated in Section 4.2, available observation data consist of groundwater hydraulic head time series at 16 observation wells and streamflow at a stream gauge located 6 km from the upstream end of the model domain. In experiment B-2, half of the hydraulic head data and the streamflow data are used to validate the updated K_a and K_s fields. To do so, the mean of the update ensembles of K_s and K_a are simulated to predict the hydraulic head at the locations and times of observed heads and the streamflow at the site of the stream gage. Figure 11 shows the comparison between the simulated and observed heads. The correlation between observed and simulated head is r = 0.99 and L_1 = 1.50, indicating good performance of the inversion process.

In a similar manner, the simulated and observed stream flow at the stream gage is shown in Figure 12. Figure 12a compares monthly simulated and observed stream flow rates. A general agreement between the two time-series is observed, with r = 0.685 (Figure 12b) and $L_1 = 4.2 \times 10^5$. Streamflow estimation could be significantly improved if the stream gage was located further downstream within the study area. Since the stream gage is located only 6 km from the upstream end, the updated K_s and K_a fields do not have a strong influence on surface water – groundwater exchange rates.

To explore the impact of not calibrating the spatial variability of streambed K_s, the ES is used to recalibrate the aquifer conductivity field (K_a) assuming spatially constant streambed K_s equal to the posterior average streambed conductivity ($\overline{K_s}$) estimated in experiment B1. In this calibration experiment, the forecast is achieved by simulating an ensemble of spatially variable K_a realizations, whereas the streambed K_s is assumed to be spatially constant and deterministic ($\ln(\overline{K_s}) \approx -0.008$). The recalibrated conductivity field $K_a^{'}$ is compared to the conductivity field K_a estimated in experiment B1 (Figure 7a). The spatial variability of the difference between the two fields ($\ln(K_a) - \ln(K_a^{'})$) is shown in Figure 13a, whereas Figure 13b compares between the observed hydraulic heads and the simulated heads using $K_a^{'}$ field. Erroneously disregarding the calibration of the K_s field produces a suboptimal estimation of K_a field that compensates for this error and still minimizes the calibration residual error. As a result, the correlation between the simulated heads and observed heads decreased from r = 0.99 for the case wherein the spatial variability of K_s is calibrated to r = 0.97 where K_s calibration is disregarded. It is worth noting that disregarding the calibration of K_s can be seen as adopting a different parametrization scheme for the unknown parameters that still minimizes the calibration residual error (The equifinality of inverse problem (Beven, 2001)).

6. Summary and Conclusions

This study implements data assimilation of groundwater level measurements using the Ensemble Smoother to estimate the spatial heterogeneity of both spatially-varying streambed and hydraulic conductivity along a 35.6 km reach of the South Platte River in northeastern Colorado. The two fields were parameterized using cellblocks with sizes of 304.8 m square. Two numerical experiments were conducted to explore the performance of data assimilation: (1) assimilating synthetic data and (2) assimilating historical groundwater levels from 16 observation wells. In the synthetic experiment, assimilated groundwater head measurements were obtained from known streambed and aquifer hydraulic conductivity fields, with measurements having the same spatial locations and temporal frequencies as the historical data. In assimilating the historical head data, half of the available groundwater level measurements are used in the assimilation, while the other half and streamflow measurements are used to evaluate the accuracy of the estimated fields.

Results show that the Ensemble Smoother reproduces the synthetic streambed and aquifer hydraulic conductivity fields with very good agreement to the reference fields. In assimilation of historical data, results show that simulated groundwater levels and stream flow rates using the estimated streambed and aquifer hydraulic conductivity fields are in reasonably good agreement with observed data. The posterior ensemble means of estimated K_s and K_a fields were used to estimate the spatial variability of stream-aquifer flux exchange, which show high degree of spatial variability. While applying data assimilation to estimate the parameters of groundwater systems is still limited in practice, this work shows that the approach can provide a reliable and computationally affordable inversion tool and the methods described in this paper can be applied to other stream-aquifer systems.

References

Alzraiee, A. H., D. Baú, and A. Elhaddad. 2014. "Estimation of Heterogeneous Aquifer Parameters Using Centralized and Decentralized Fusion of Hydraulic Tomography Data." Hydrology and Earth System Sciences 18 (8): 3207–23. doi:10.5194/hess-18-3207-2014.

Avery, C. (1994), "Interaction of ground water with the Rock River near Byron", Illinois. U.S. Geological Survey Water-Resources Investigations Report 94-4034.

Bailey, R.T., and D.A. Baù (2011), "Estimating spatially-variable first-order rate constants in groundwater reactive transport systems", J. Cont. Hydrol., 122, 104-121.

Bailey, R.T., Baù, D., and T.K. Gates (2013), "Estimating spatially-variable rate constants of denitrification in an irrigated agricultural groundwater system using an Ensemble Smoother". Journal of Hydrology, 468-469, 188-202.

Becker, M.W., Georgian, T., Ambrose, H., Sinischalchi, J., and K. Fredrick (2004), "Estimating flow and flux of ground water discharge using water temperature and velocity". J. Hydrology 296, 221-233.

Beven, K. 2001. " How far can we go in distributed hydrological modelling?", Hydrol. Earth Syst. Sci., 5, 1-12, doi:10.5194/hess-5-1-2001, 2001.

Burgers, G., P.J. van Leeuwen, and G. Evensen (1998), Analysis scheme in the Ensemble Kalman Filter, Mon. Weather Rev., 126, 1719-1724.

Calver, A. 2001. "Riverbed Permeabilities: Information from Pooled Data." Ground Water 39 (4): 546–53.

Cardenas, M. Bayani, J. L. Wilson, and V. A. Zlotnik. 2004. "Impact of Heterogeneity, Bed Forms, and Stream Curvature on Subchannel Hyporheic Exchange." Water Resources Research 40 (8): W08307. doi:10.1029/2004WR003008.

Cardenas, M. Bayani, and Vitaly A. Zlotnik. 2003. "Three-Dimensional Model of Modern Channel Bend Deposits." Water Resources Research 39 (6): 1141. doi:10.1029/2002WR001383.

Cey, Edwin E., David L. Rudolph, Ramon Aravena, and Gary Parkin. 1999. "Role of the Riparian Zone in Controlling the Distribution and Fate of Agricultural Nitrogen near a Small Stream in Southern Ontario." Journal of Contaminant Hydrology 37 (1–2): 45–67. doi:10.1016/S0169-7722(98)00162-4.

Colorado Geological Survey. 2003. Ground Water Atlas of Colorado. Special Publication 53.

CDM Smith (2013) "South Platte Decision Support System Alluvial Groundwater Model Report" , Prepared for the Colorado Water Conservation Board and Colorado Division of Water Resources.

Chen, Xunhong, and Longcang Shu. 2002. "Stream-Aquifer Interactions: Evaluation of Depletion Volume and Residual Effects from Ground Water Pumping." Ground Water 40 (3): 284–90. doi:10.1111/j.1745-6584.2002.tb02656.x.

Chen, Yan, and Dongxiao Zhang. 2006. "Data Assimilation for Transient Flow in Geologic Formations via Ensemble Kalman Filter." Advances in Water Resources 29 (8): 1107–22. doi:10.1016/j.advwatres.2005.09.007.

Duff, J.H., Toner, B., Jackman, A.P., Azanzino, R.J., and F.J. Triska (2000), Determination of groundwater discharge into a sand and gravel bottom river: A comparison of chloride dilution and seepage meter techniques. Verh. Internat. Verein. Limnol. 27, 406-411.

Evensen, Geir. 1994. "Sequential Data Assimilation with a Nonlinear Quasi-Geostrophic Model Using Monte Carlo Methods to Forecast Error Statistics." Journal of Geophysical Research: Oceans 99 (C5): 10143–62. doi:10.1029/94JC00572.

Fleckenstein, J.H., Niswonger, R.G., and G.E. Fogg (2006), River-aquifer interactions, geologic heterogeneity, and low-flow management. Ground Water 44, 837-52.

Fleckenstein, J.H., S. Krause, D.M. Hannah, F. Boano. Groundwater-surface water interactions: New methods and models to improve understanding of processes and dynamics. 2010. Advances in Water Resources 33: 1291-1295.

Frei, S., Fleckenstein, J.H., Kollet, S.J., and R.M. Maxwell (2009), Patterns and dynamics of river-aquifer exchange with variably-saturated flow using a fully-coupled model. J. Hydrology 375, 383-393.

Fryar, A.E., Wallin, E.J., and D.L. Brown (2000), Spatial and temporal varaibiltiy in seepage between a contaminated aquifer and tributaries to the Ohio River. Ground Water Monitoring and Remediation 20(3), 129-146.

Genereux, David P., Scott Leahy, Helena Mitasova, Casey D. Kennedy, and D. Reide Corbett. 2008. “Spatial and Temporal Variability of Streambed Hydraulic Conductivity in West Bear Creek, North Carolina, USA.” Journal of Hydrology 358 (3–4): 332–53. doi:10.1016/j.jhydrol.2008.06.017.

Glover, Robert E., and Glenn G. Balmer. 1954. “River Depletion Resulting from Pumping a Well near a River.” Eos, Transactions American Geophysical Union 35 (3): 468–70. doi:10.1029/TR035i003p00468.

Hantush, M.M., and M.A. Marino (1997), Estimation of spatially variable aquifer hydraulic properties using Kalman filtering. J. Hydraul. Engrg. ASCE, 123(11), 1027-1035.

Harbaugh, Arlen W., Edward R. Banta, Mary C. Hill, and Michael G. McDonald. 2000. MODFLOW-2000, the US Geological Survey Modular Ground-Water Model: User Guide to Modularization Concepts and the Ground-Water Flow Process. US Geological Survey Reston, VA. http://funnel.sfsu.edu/students/dotsona/geosci/courses/G700/Documents-Manuals-PDFs/DOC3_MODFLOW2000_ModConcepts_GWFlowProcess_ofr00-92.pdf.

Hatch, Christine E., Andrew T. Fisher, Chris R. Ruehl, and Greg Stemler. 2010. “Spatial and Temporal Variations in Streambed Hydraulic Conductivity Quantified with Time-Series Thermal Methods.” Journal of Hydrology 389 (3–4): 276–88. doi:10.1016/j.jhydrol.2010.05.046.

Hendricks Franssen, H. J., and W. Kinzelbach. 2008. “Real-Time Groundwater Flow Modeling with the Ensemble Kalman Filter: Joint Estimation of States and Parameters and the Filter Inbreeding Problem.” Water Resources Research 44 (9): W09408. doi:10.1029/2007WR006505.

Hendricks Franssen, H. J., H. P. Kaiser, U. Kuhlmann, G. Bauser, F. Stauffer, R. Müller, and W. Kinzelbach. 2011. “Operational Real-Time Modeling with Ensemble Kalman Filter of Variably Saturated Subsurface Flow Including Stream-Aquifer Interaction and Parameter Updating.” Water Resources Research 47 (2): W02532. doi:10.1029/2010WR009480.

Hussein, Maged, and Franklin W. Schwartz. 2003. “Modeling of Flow and Contaminant Transport in Coupled Stream-Aquifer Systems.” Journal of Contaminant Hydrology 65 (1-2): 41–64. doi:10.1016/S0169-7722(02)00229-2.

Jenkins, C. T. 1968. “Techniques for Computing Rate and Volume of Stream Depletion by Wellsa.” Ground Water 6 (2): 37–46. doi:10.1111/j.1745-6584.1968.tb01641.x.

Kalbus, E., Schmidt, C., Bayer-Raich, M., Leschik, S., Reinstorf, F., Balcke, G., and Schirmer, M. (2007), New methodology to investigate potential contaminant mass fluxes at the stream-aquifer interface by combining integral pumping tests and streambed temperatures, Environ. Pollut., 148, 808–816.

Kalbus, E., C. Schmidt, J. W. Molson, F. Reinstorf, and M. Schirmer. 2009. "Influence of Aquifer and Streambed Heterogeneity on the Distribution of Groundwater Discharge." Hydrol. Earth Syst. Sci. 13 (1): 69–77. doi:10.5194/hess-13-69-2009.

Keery, J., Binley, A., Crook, N., and J.W.N. Smith (2007), Temporal and spatial variability of groundwater-surface water fluxes: development and application of an analytical method using temperature time series. J. Hydrology 336, 1-16.

Krause, S., Bronstert, A., and E. Zehe (2007), Groundwater-surface water interactions in a North German lowland floodplain – Implications for the river discharge dynamics and riparian water balance. J. Hydrology 347, 404-417.

Kurtz, W., Hendricks Franssen, H.-J., and H. Vereecken (2012), Identification of time-variant river bed properties with the ensemble Kalman filter. Water Res. Research 48, W10534, doi:10.1029/2011WR011743.

Kurtz, W., H.-J. Hendricks Franssen, P. Brunner, and H. Vereecken. 2013. "Is High-Resolution Inverse Characterization of Heterogeneous River Bed Hydraulic Conductivities Needed and Possible?" Hydrol. Earth Syst. Sci. 17 (10): 3795–3813. doi:10.5194/hess-17-3795-2013.

Kurtz, W., H.-J. Hendricks Franssen, H.-P. Kaiser, and H. Vereecken (2014),Joint assimilation of piezometric heads and groundwater temperatures for improved modeling of river-aquifer interactions, Water Resour. Res., 50, 1665–1688, doi:10.1002/2013WR014823.

Lackey, G., Neupauer, R.M., and J. Pitlick (2015), Effects of streambed conductance on stream depletion. Water 7, 271-287.

Laloy, Eric, Bart Rogiers, Jasper A. Vrugt, Dirk Mallants, and Diederik Jacques. 2013. "Efficient Posterior Exploration of a High-Dimensional Groundwater Model from Two-Stage Markov Chain Monte Carlo Simulation and Polynomial Chaos Expansion." Water Resources Research 49 (5): 2664–82. doi:10.1002/wrcr.20226.

Loheide, Steven P., and Steven M. Gorelick. 2006. "Quantifying Stream−Aquifer Interactions through the Analysis of Remotely Sensed Thermographic Profiles and In Situ Temperature Histories." Environmental Science & Technology 40 (10): 3336–41. doi:10.1021/es0522074.

Liu, G., Chen, Y., and D. Zhang (2008), Investigation of flow and transport processes at the MADE site using ensemble Kalman filter. Adv. Water Resour. 31, 975–986.

Marsily, Ghislain De. 1986. Quantitative Hydrogeology: Groundwater Hydrology for Engineers. 1 edition. San Diego: Academic Press.

Miller, Calvin D., Deanna Durnford, Mary R. Halstead, Jon Altenhofen, and Val Flory. 2007. “Stream Depletion in Alluvial Valleys Using the SDF Semianalytical Model.” Ground Water 45 (4): 506–14. doi:10.1111/j.1745-6584.2007.00311.x.

Morway, E. D., Gates, T. K., and Niswonger, R. G. (2013), Appraising options to enhance shallow groundwater table and flow conditions over regional scales in an irrigated alluvial aquifer system. J. Hydrology, 495: 216-237.

Nyquist, J.E., Freyer, P.A., and L. Toran (2008), Stream bottom resistivity tomography to map ground water discharge. Ground Water 46(4), 561-569.

Paulsen, R.J., Smith, C.F., O’Rourke, D., and T.-F. Wong (2001), Development and evaluation of an ultrasonic ground water seepage meter. Ground Water 39(6), 904-911.

Prudic, David E., Leonard F. Konikow, and Edward R. Banta. 2004. A New Streamflow-Routing (SFR1) Package to Simulate Stream-Aquifer Interaction with MODFLOW-2000. US Department of the Interior, US Geological Survey.

Rosenberry, Donald O., and John Pitlick. 2009. “Effects of Sediment Transport and Seepage Direction on Hydraulic Properties at the Sediment–water Interface of Hyporheic Settings.” Journal of Hydrology 373 (3–4): 377–91. doi:10.1016/j.jhydrol.2009.04.030.

Rossi, P., A. De Carvalho-Dill, I. Müller, and M. Aragno. 1994. “Comparative Tracing Experiments in a Porous Aquifer Using Bacteriophages and Fluorescent Dye on a Test Field Located at Wilerwald (Switzerland) and Simultaneously Surveyed in Detail on a Local Scale by Radio-Magneto-Tellury (12–240 kHz).” Environmental Geology 23 (3): 192–200. doi:10.1007/BF00771788.

Schmidt, C., Kalbus, E., Martienssen, M., and Schirmer, M. (2008), The influence of heterogeneous groundwater discharge on the timescales of contaminant mass flux from streambed sediments – field evidence and long-term predictions, Hydrol. Earth Syst. Sci. Discuss., 5, 971–1001, 2008, http://www.hydrol-earth-syst-sci-discuss.net/5/971/2008/.

Silliman, S.E. and D.F. Booth (1993), Analysis of time-series measurements of sediment temperature for identification of gaining vs. losing portions of Juday Creek, Indiana. J. Hydrology 146, 131-148.

Silliman, S.E., Ramirez, J., and R.L. McCabe (1995), Quantifying downflow through creek sediments using temperature time series: One-dimensional solution incorporating measured surface temperature. J. Hydrology 167, 99-119.

Sophocleous, Marios, Antonis Koussis, J. L. Martin, and S. P. Perkins. 1995. “Evaluation of Simplified Stream-Aquifer Depletion Models for Water Rights Administration.” Ground Water 33 (4): 579–88. doi:10.1111/j.1745-6584.1995.tb00313.x.

Springer, Abraham E., William D. Petroutson, and Betsy A. Semmens. 1999. “Spatial and Temporal Variability of Hydraulic Conductivity in Active Reattachment Bars of the Colorado River, Grand Canyon.” Ground Water 37 (3): 338–44. doi:10.1111/j.1745-6584.1999.tb01109.x.

van Leeuwen, P.J., and G. Evensen (1996), Data assimilation and inverse methods in terms of probabilistic formulation. Mon. Weather Rev., 124, 2898-2913.

Vogt, T., Schneider, P., Hahn-Woernle, L., and O.A. Cirpka (2010), Estimation of seepage rates in a losing stream by means of fiber-optic high-resolution vertical temperature profiling. J. Hydrology 380, 154-164.

Woessner, William W. 2000. “Stream and Fluvial Plain Ground Water Interactions: Rescaling Hydrogeologic Thought.” Ground Water 38 (3): 423–29. doi:10.1111/j.1745-6584.2000.tb00228.x.

Table 1. Groundwater Model Setting and Properties of the Geostatistical Model for Hydraulic Parameters.

Properties of Finite Difference Grid	
Horizontal Domain Dimensions [x,y]	[30 km,30 km]
Saturated Thickness [z]	15 m - 88 m
Rows, Columns, and Layers	[100,100,1]
Number of Active Cells	3461
Simulation Times	
Simulated Period	2000 to 2006
Steady State stress period	One month (1/2000)
Transient State Stress Period	84 Months (7 years)
Time step	1 day
Boundary Conditions	
Upper Boundary Condition (Fig. 2)	Variable flux for each stress period.
lower Boundary Condition (Fig. 2)	Variable flux for each stress period.
Northern Side Boundary Condition (Fig. 2)	Variable flux for each stress period.
Southern Side Boundary Condition (Fig. 2)	Variable flux for each stress period.
Initial Boundary Condition (Fig. 2)	Interpolated groundwater table measurements for January 2000
Geostatistical Properties of Aquifer Parameters	
Log(K_a) - 2D isotropic field [$\mu_y, \sigma_y^2, \lambda_y$]	[5,1.5,4000m]
Log(K_s) - 1D field [$\mu_z, \sigma_z^2, \lambda_z$]	[0.1,0.1,2000m]
Sy	Constant Value (0.20)

Table 2. Data Assimilation Experiments and Cross-validation of Estimated Parameters

Experiment	Description	Data Used	Ensemble Size
A	Synthetic Data Assimilation	Synthetic Head Data	500 realizations
B	B-1 Assimilation of Actual Field Data	Actual Head Data at 16 Observation wells at 2472 different times.	500 realizations
	B-2 Cross-Validation of Estimated Parameters.	• Actual Head Data at 16 Observation wells at 2472 different times. • Month Stream flow Data for the period 2000 to 2006.	N/A

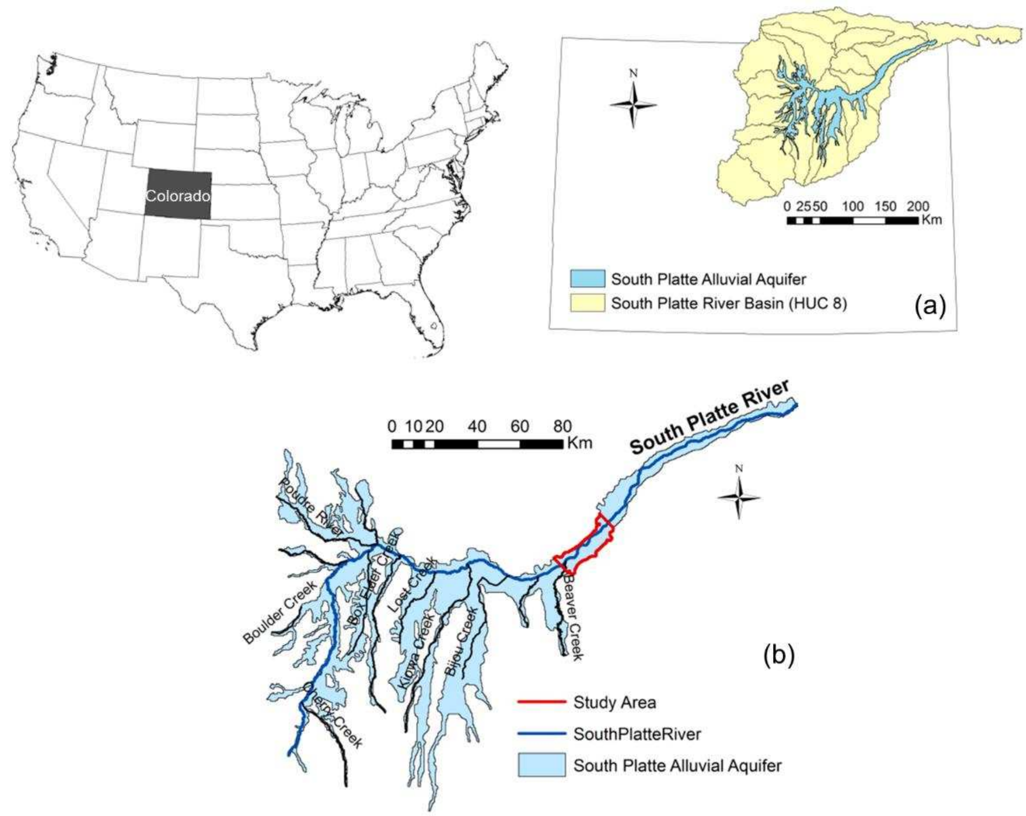

Figure 1. Regional stream-aquifer system of the South Platter River Basin in northeastern Colorado is shown in panel (a). The alluvial aquifer and local study area are shown in panel (b).

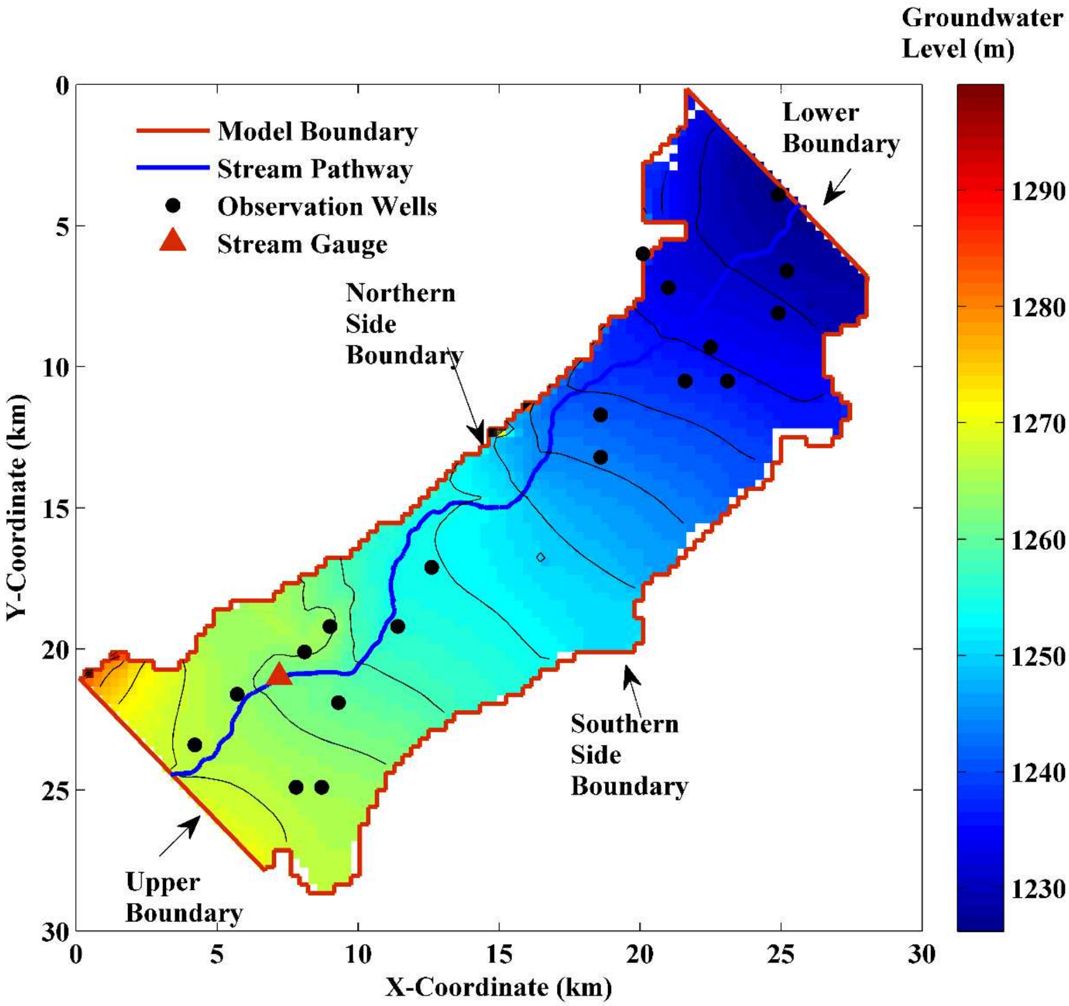

Figure 2. Model Boundaries, stream reach, observation wells, and stream gauge within the study area. The simulated groundwater hydraulic head is shown for December 2006.

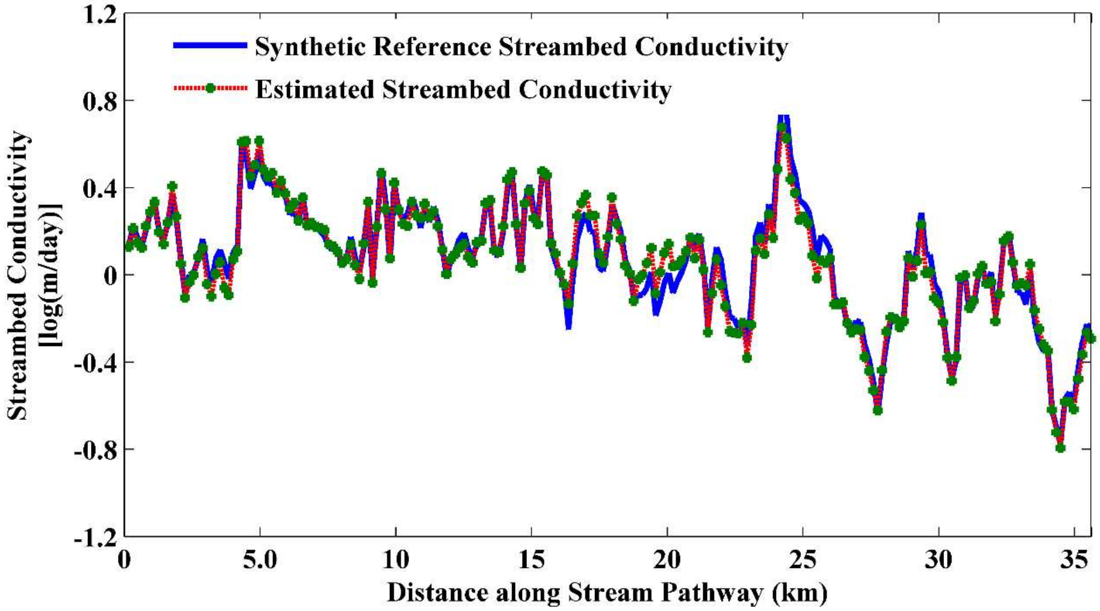

Figure 3. Comparison between the reference streambed conductivity field and the mean of the updated ensemble of streambed conductivity field using synthetic hydraulic head data only.

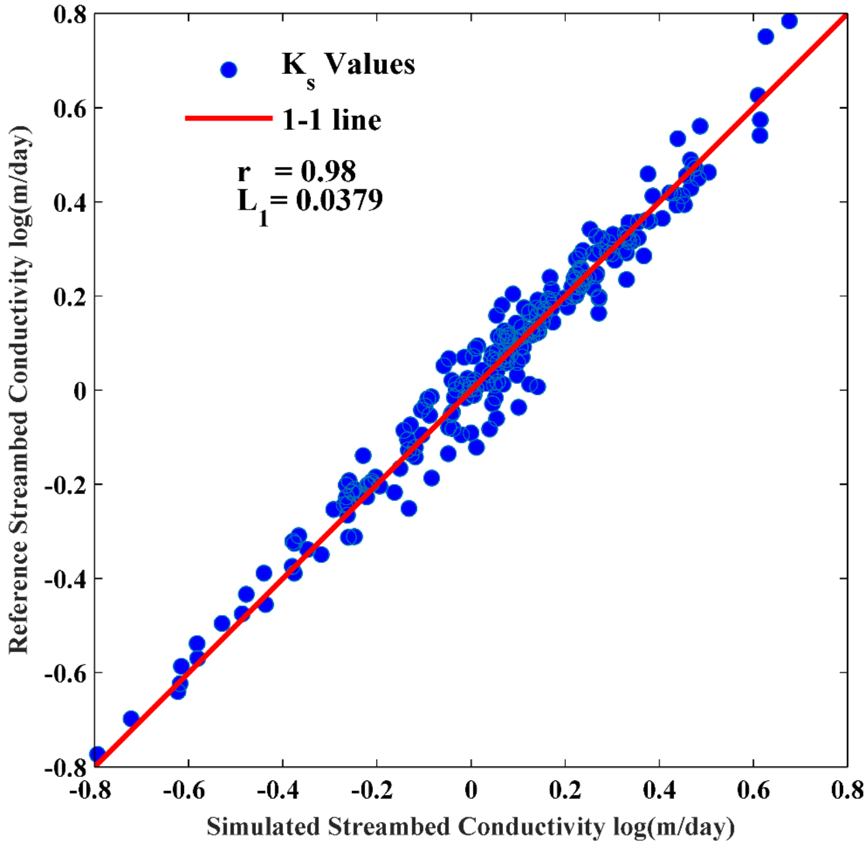

Figure 4. Scatter plot comparing the reference streambed K_s field values and the mean of the updated ensemble of streambed K_s values estimated by assimilating synthetic hydraulic head data.

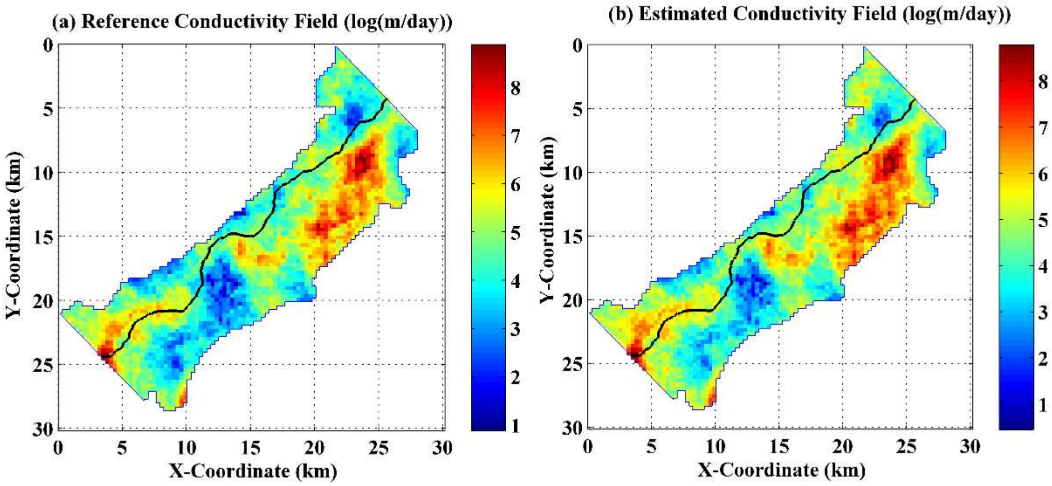

Figure 5. Comparison between (a) the reference aquifer K field and (b) the mean of the updated ensemble of aquifer K fields, by assimilating synthetic hydraulic head data.

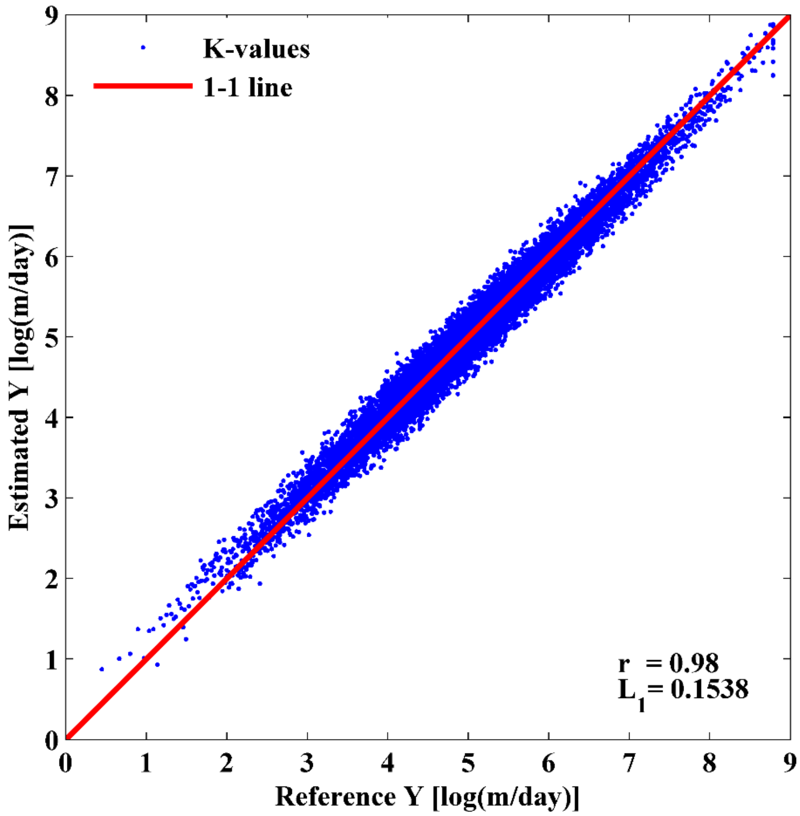

Figure 6. Scatter plot comparing the reference aquifer K field values and the mean of updated ensemble of aquifer K values, by assimilating synthetic hydraulic head data.

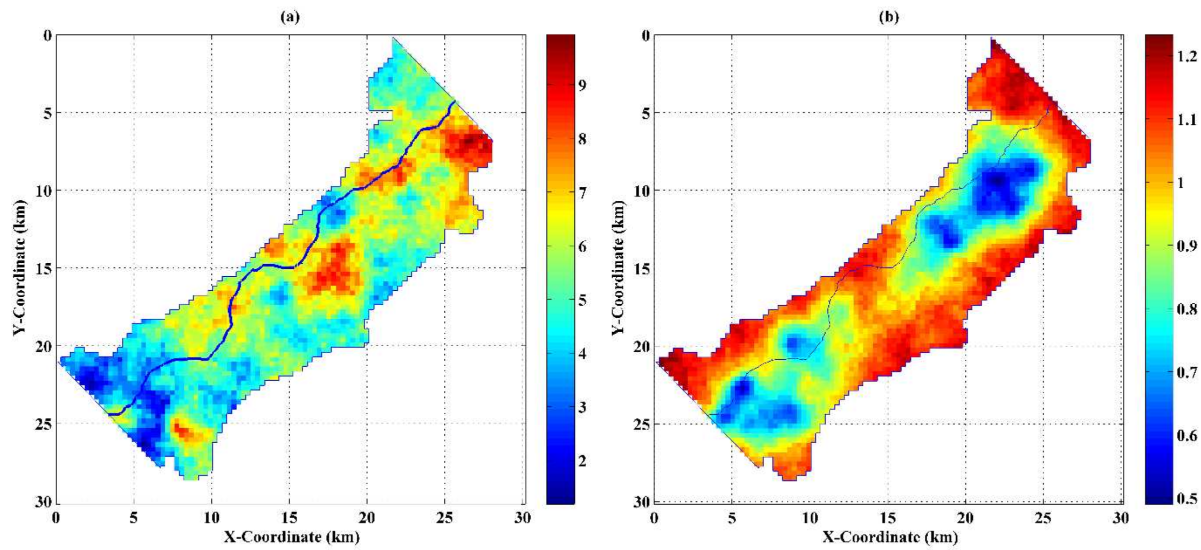

Figure 7. Panel (a) shows the ensemble mean of the hydraulic conductivity (K_f) posterior ensemble (log(m/day)). Panel (b) shows the posterior standard deviation of K_f field at each local cell.

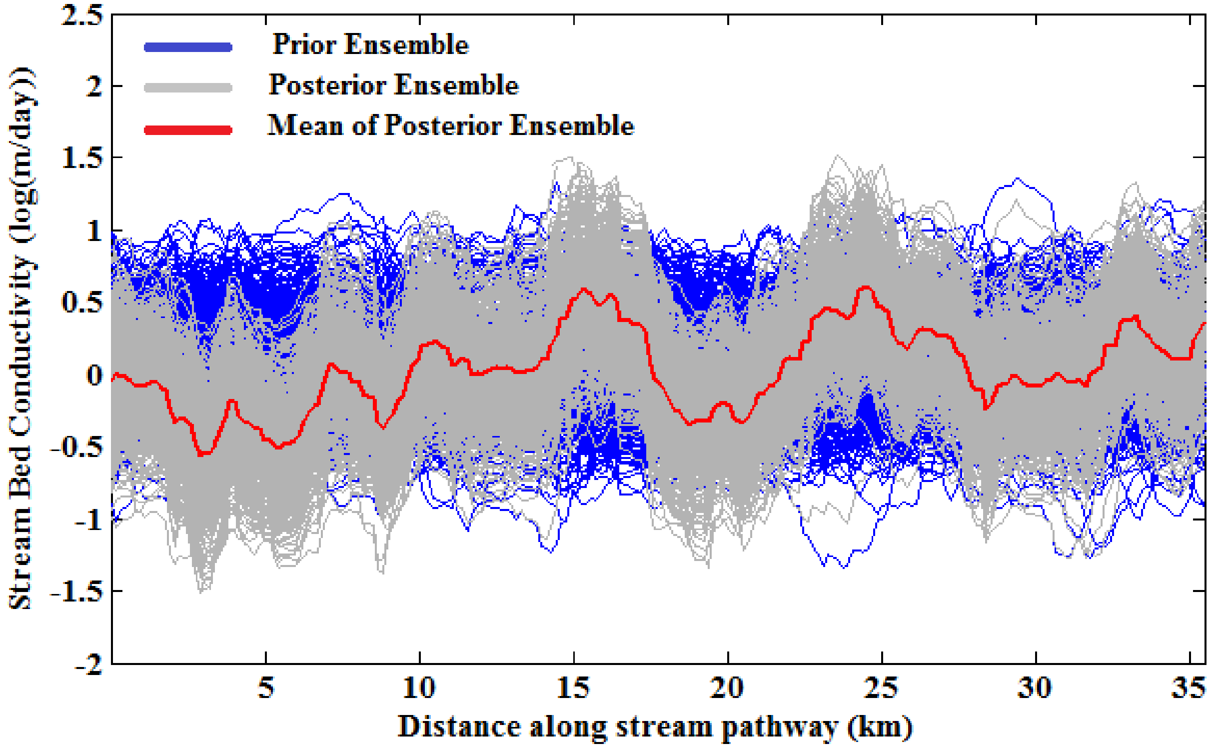

Figure 8. Prior and posterior ensembles of streambed K. The mean of the posterior ensemble is highlighted with red color.

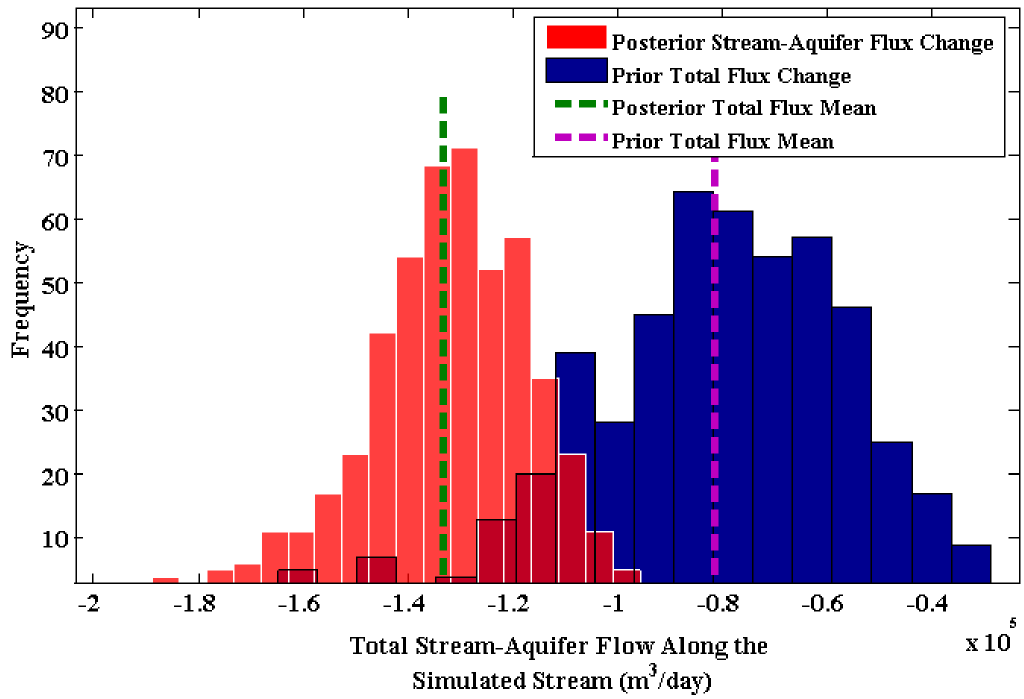

Figure 9. Shows the prior and posterior ensembles of stream-aquifer total flux exchange along the simulated stream. The means of the prior and posterior ensembles are highlighted. Negative flow rates indicate groundwater leaving the aquifer to the stream, while the positive flow rates indicate that the aquifer receives water from the stream.

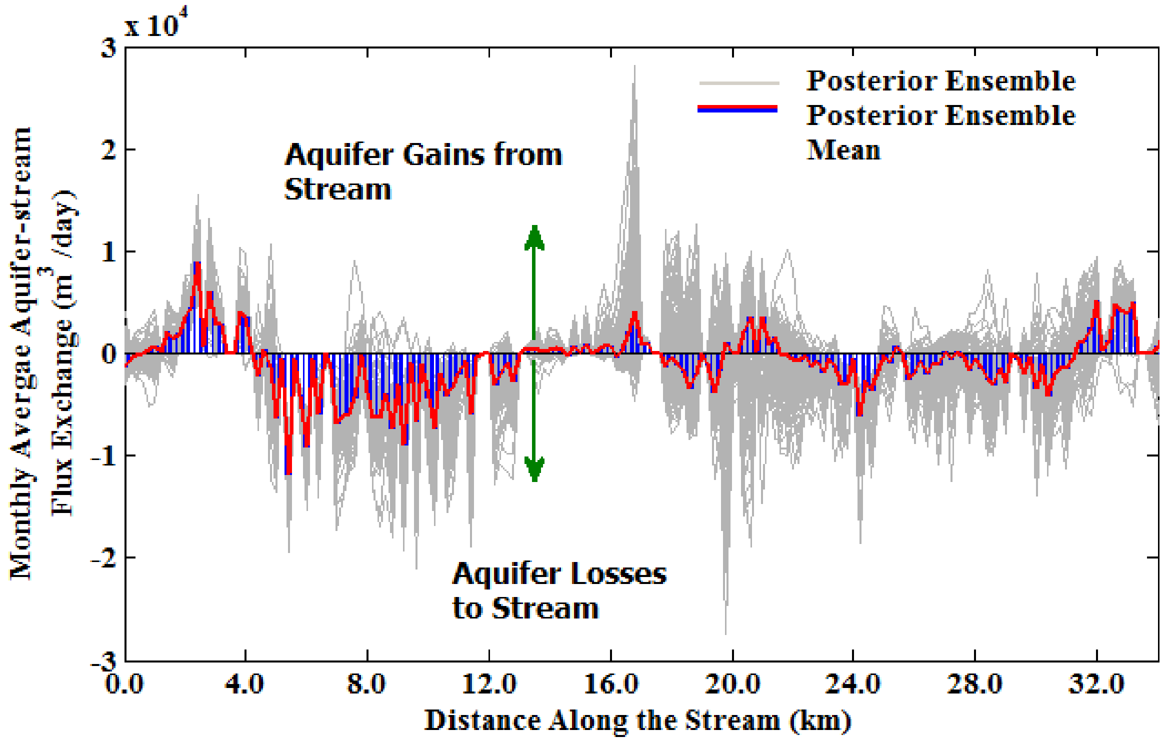

Figure 10. Shows the posterior ensembles of stream-aquifer flux exchange. The mean of the posterior ensemble is highlighted with red color. Negative flow rates indicate groundwater leaving the aquifer to the stream, while the positive flow rates indicate that the aquifer receives water from the stream.

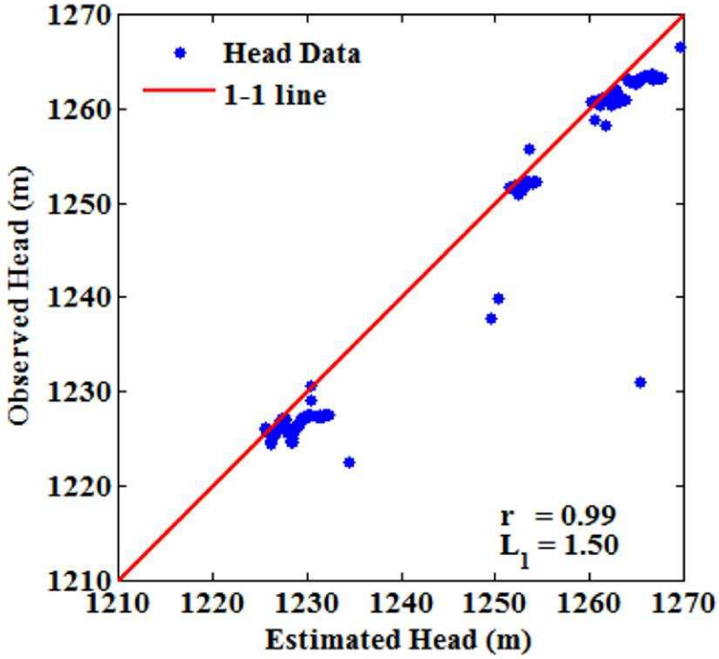

Figure 11. Scatter Plot that compares between the observed hydraulic head measurements and the simulated hydraulic head obtained by simulating the K_f and $\mathbf{K_s}$.

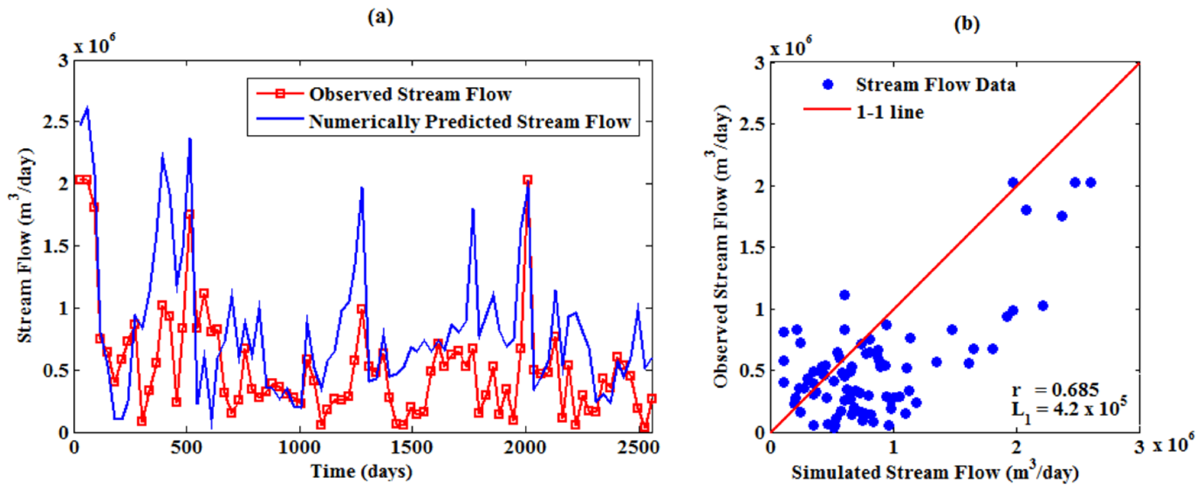

Figure 12. Panel (a) shows the simulated and observed stream flow gauges, (b) Scatter Plot that compares between the observed stream flow and the simulated stream flow obtained by simulating the estimated K_f and K_s.

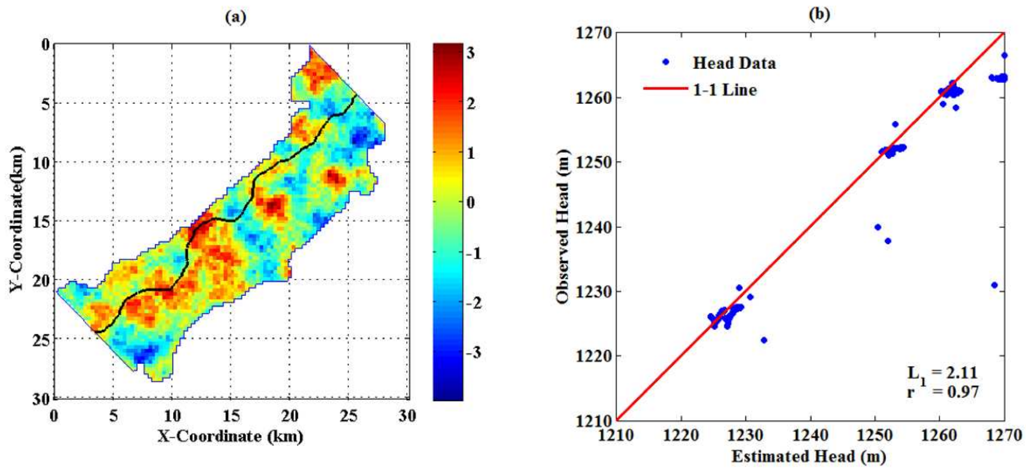

Figure 13. Panel (a) shows the spatial variability of difference between the calibrated aquifer K_a field when streambed conductivity is calibrated and aquifer $K_a^{'}$ when streambed conductivity calibration is disregarded, (b) Scatter Plot that compares between the observed hydraulic head measurements and the simulated hydraulic head obtained by simulating $K_a^{'}$.